Supplementary Information

Combined improvement of osteogenic and anti-inflammatory activities of Sr-doped bone cement modified with carboxymethyl cellulose

Xiao-Dan Li[a,c], Da-Wei Yan[a,*], Hao-Hao Ren[a], Hai-Tao Peng[d], Kun Zhao[c,*], Qi-Yi Zhang[b,*], Yong-Gang Yan

[a]College of Physics, Sichuan University, Chengdu, 610064, China.

[b]School of Chemical Engineering, Sichuan University, Chengdu, 610065, China.

[c]Institute of Fundamental and Frontier Sciences, University of Electronic Science and Technology of China, Chengdu, 611731, China.

[d]State Key Laboratory of Biotherapy, West China Hospital, Sichuan University, Chengdu, 610041, China.

*Corresponding Authors: Qi-Yi Zhang, Da-Wei Yan, and Kun Zhao.

E-mail address: qyzhang-scu@163.com, yandawei@scu.edu.cn, kzhao@uestc.edu.cn.

1. Supplementary Figures

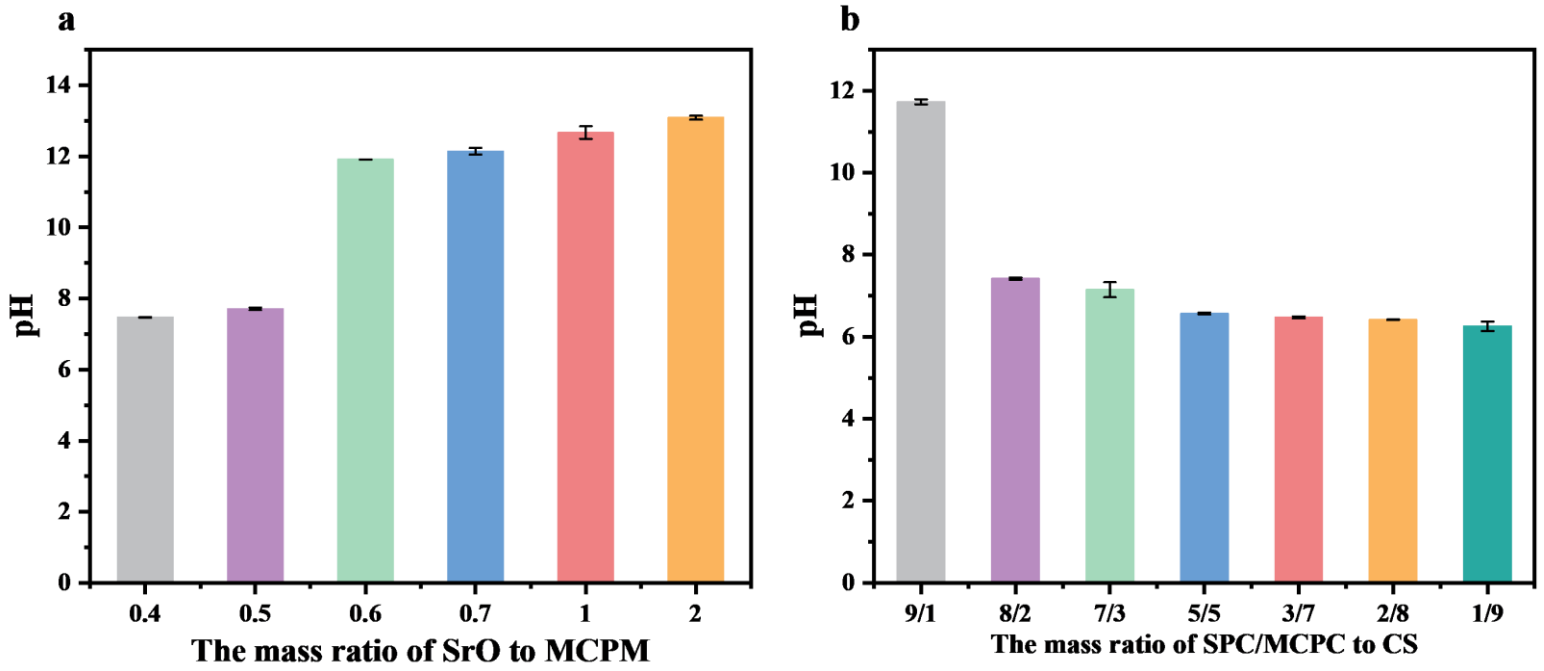

Figure S1. Screening of the optimal ratio of composite bone cement.

The optimal ratio of SrO and MCPM: After screening the pH values of different mass ratios of SrO and MCPM cement samples in PBS solution, the optimal mass ratio of SrO to MCPM is 3:5 because its pH is close to 12, allowing a pH buffer for the subsequent CS with a pH of about 4.5.

The optimal ratio of SrO/MCPM and CS: To promote the degradation of the composite bone cement and provide an adequate calcium source, CS was added to the SrO/MCPM composite. The optimal mass ratio of the inorganic phase was set as SrO:MCPM: CS = 3:5:2 because its pH

value is close to 7.4.

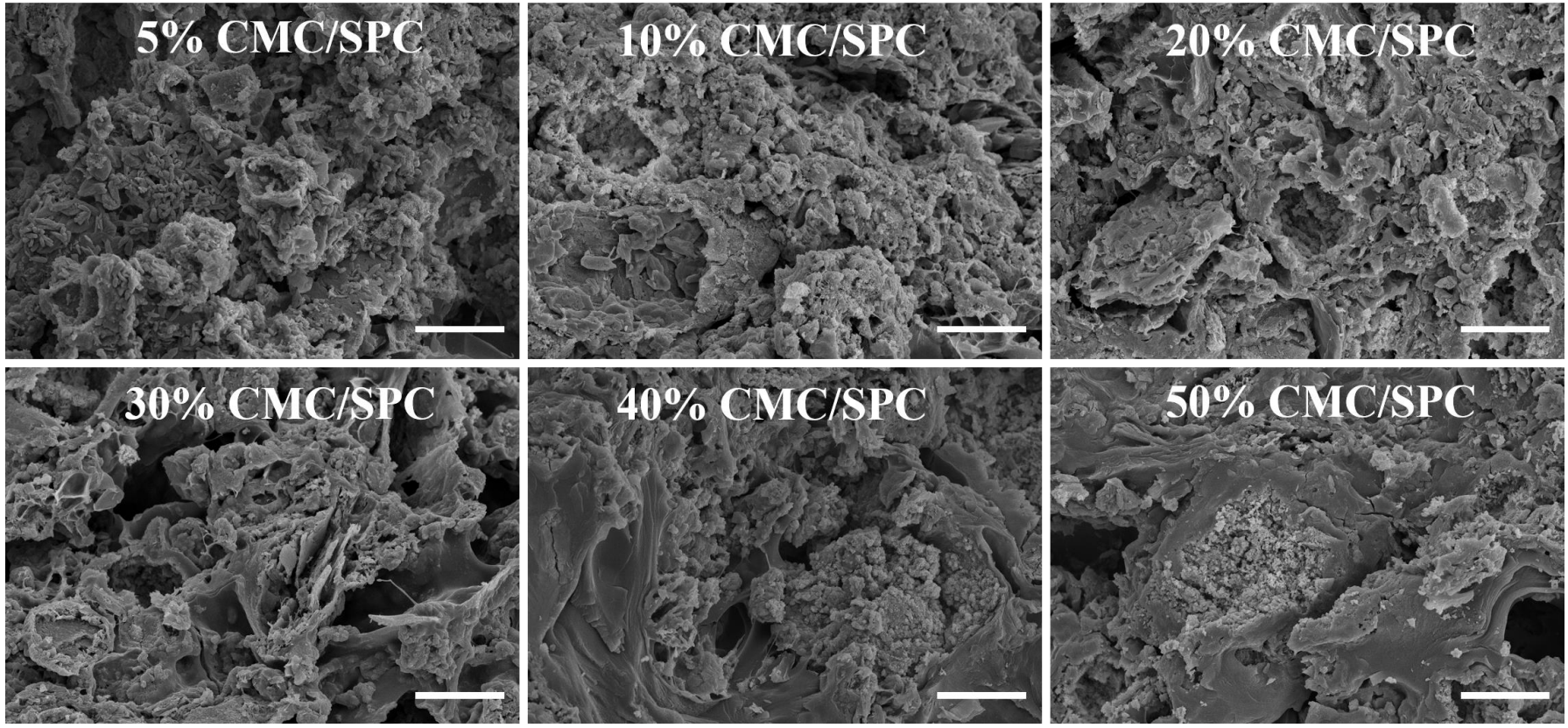

Figure S2. The cross-sectional morphology of CMC/SPC (Scale bar: 20 μm).

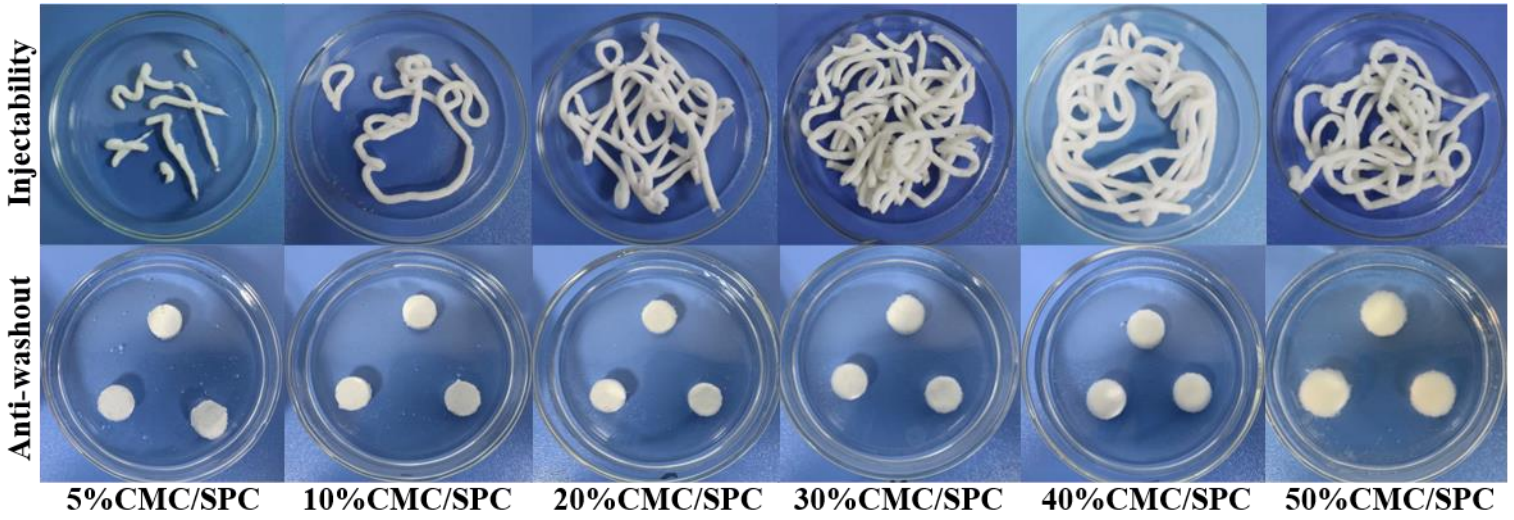

Figure S3. Digital images of injectability and anti-washout.

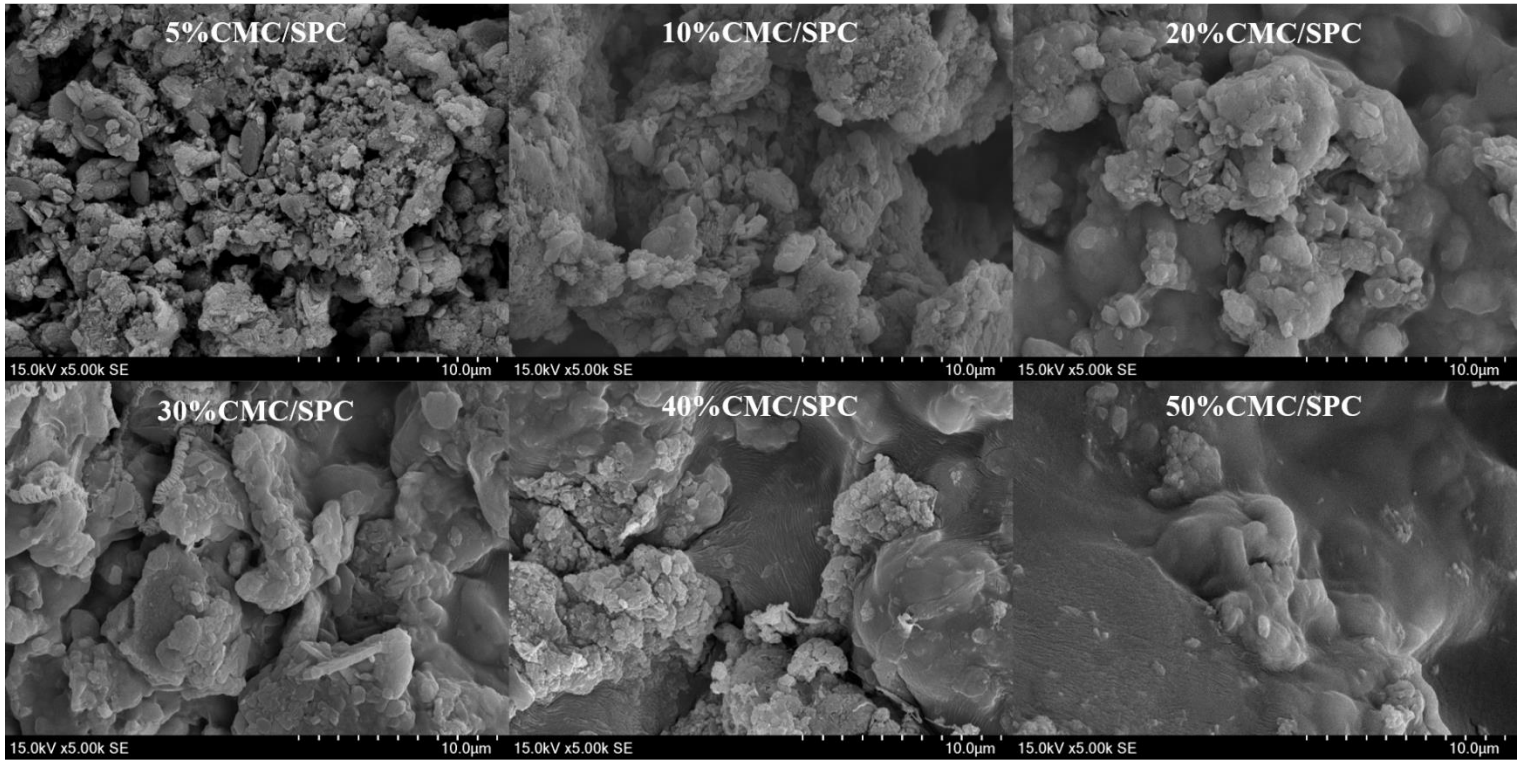

Figure S4. The surface morphology of 5-50%CMC/SPC before mineralization.

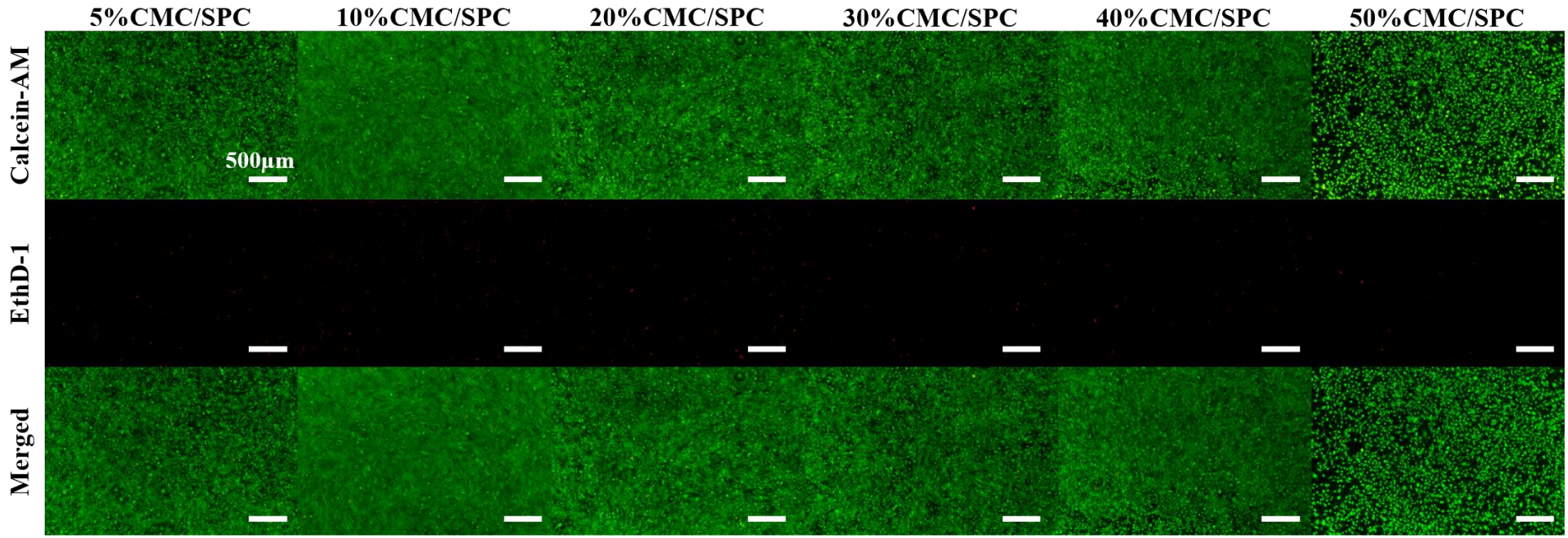

Figure S5. Fluorescent pictures of living and dead cells for 4 days (green: live cells, red: dead cells).

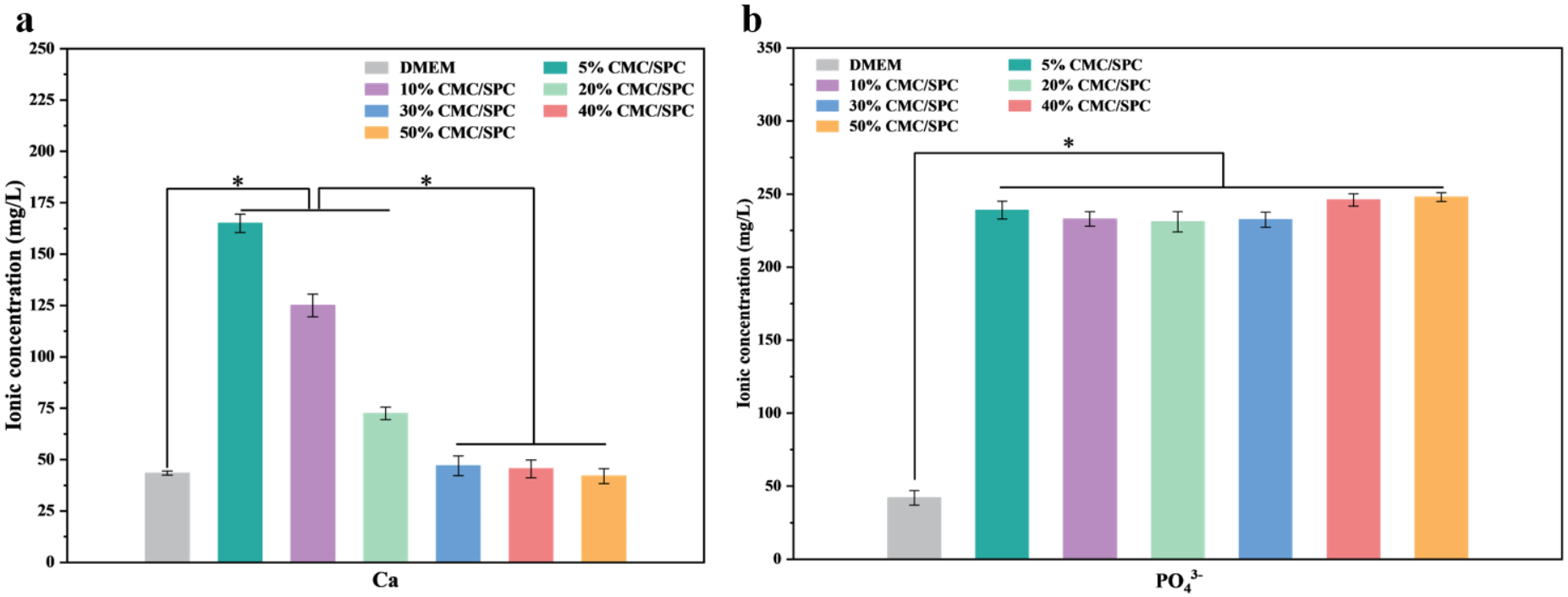

Figure S6. The Ca^{2+} and PO_4^{3-} concentrations of CMC/SPC extracts (100 mg/mL).

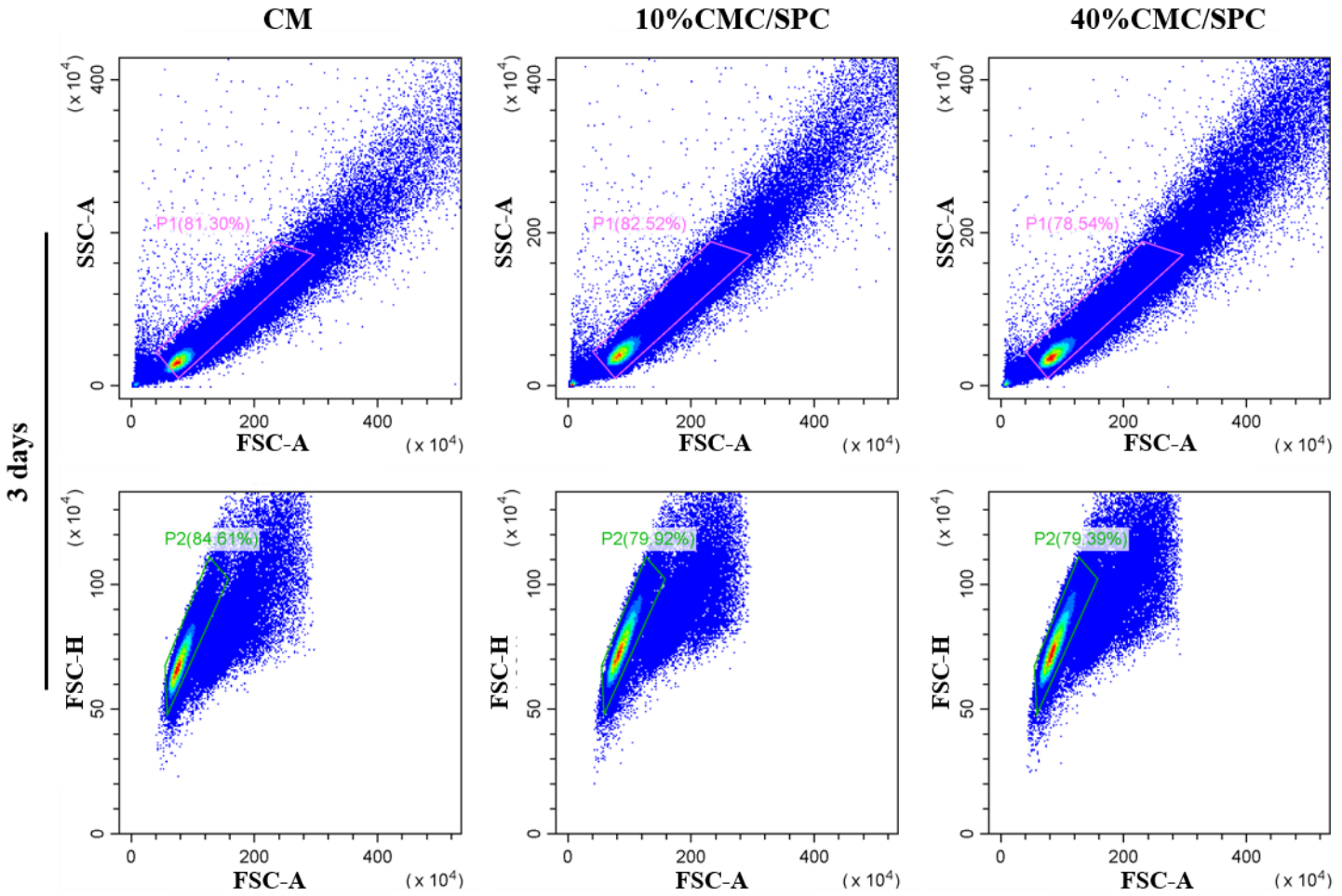

Figure S7. Flow cytometry data analysis.

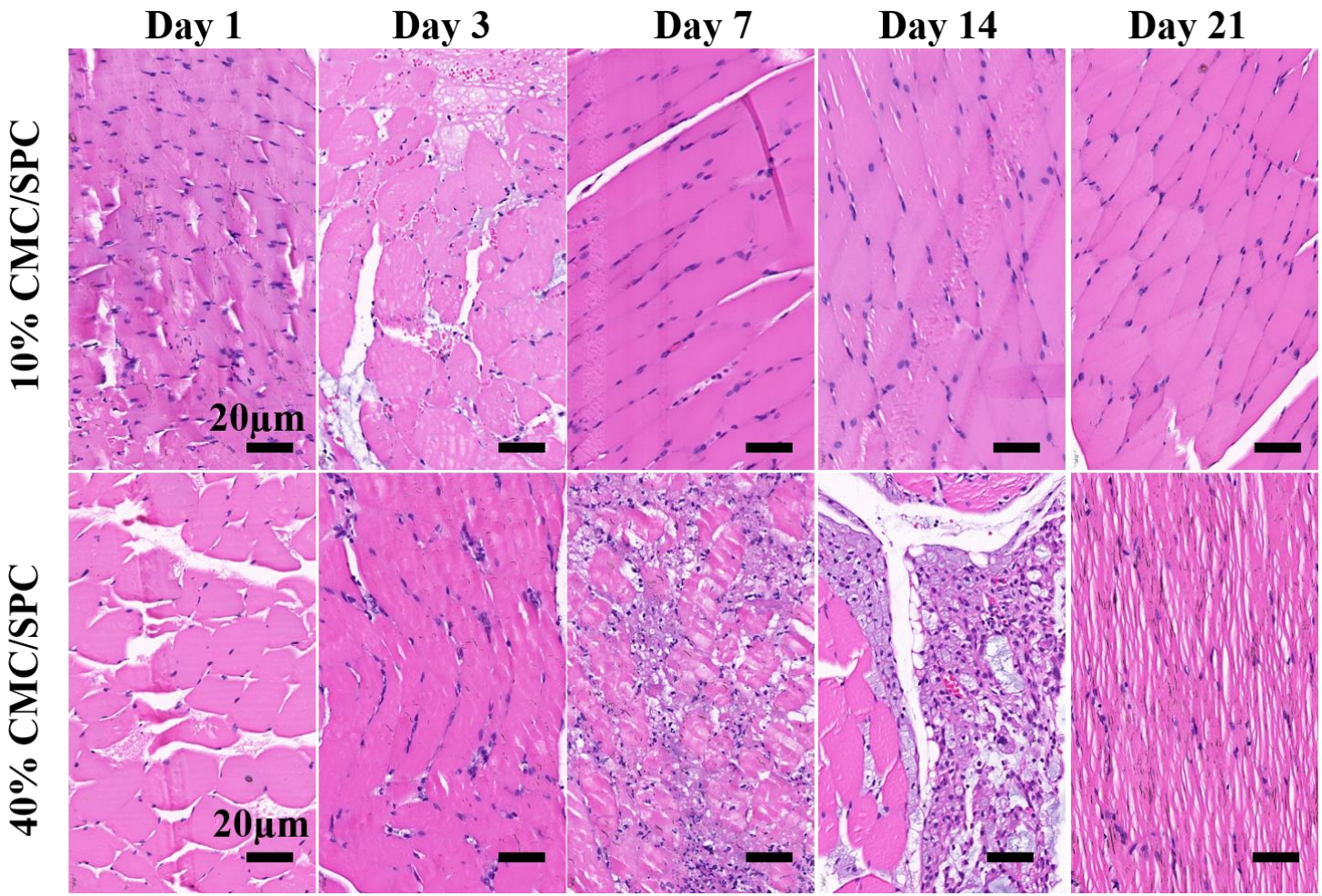

Figure S8. Representative H&E staining of implants on days 1, 3, 7, 14, and 21 after implanting in the mouse muscle.

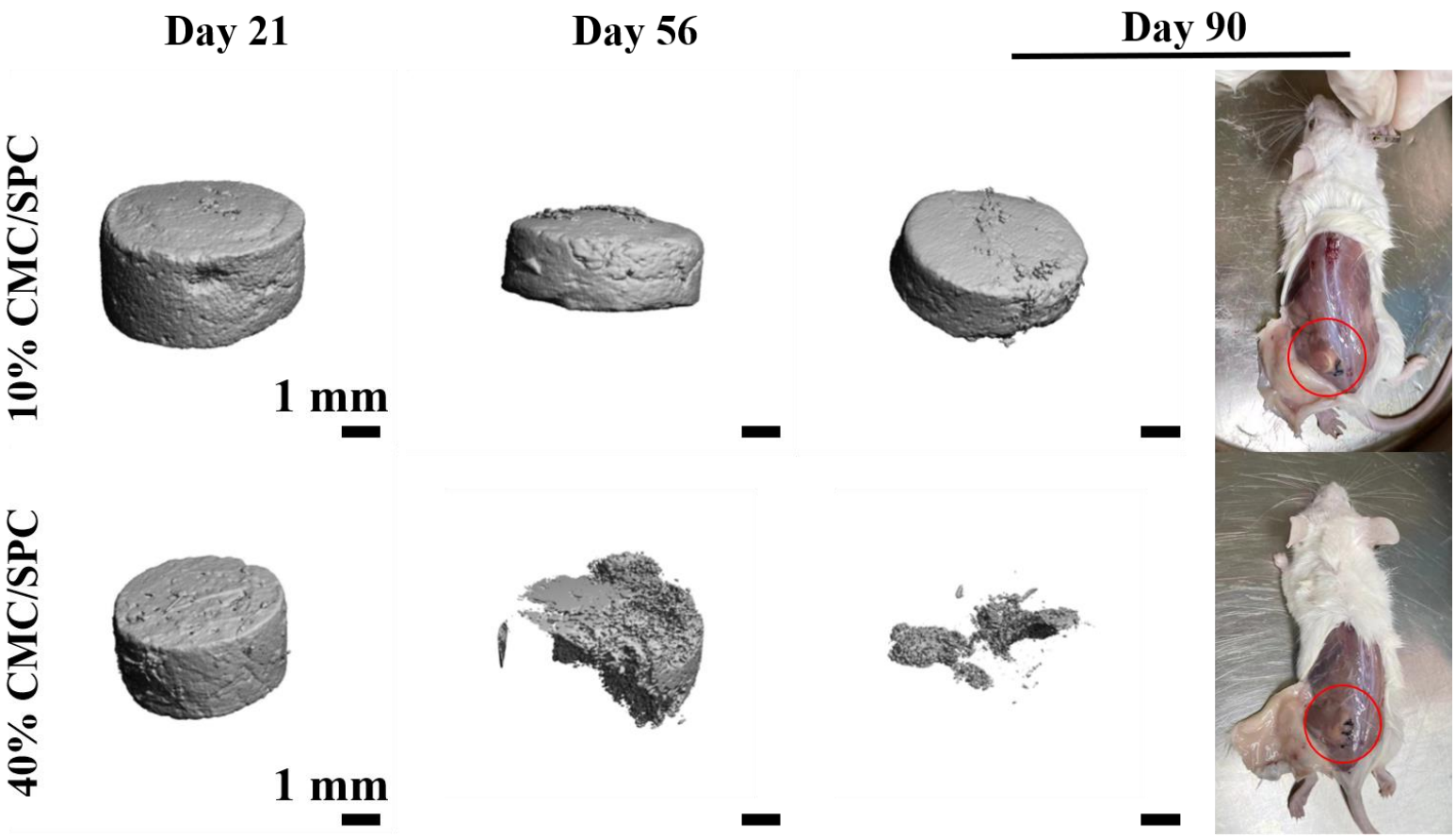

Figure S9. Representative micro-CT images on days 21, 56, and 90.

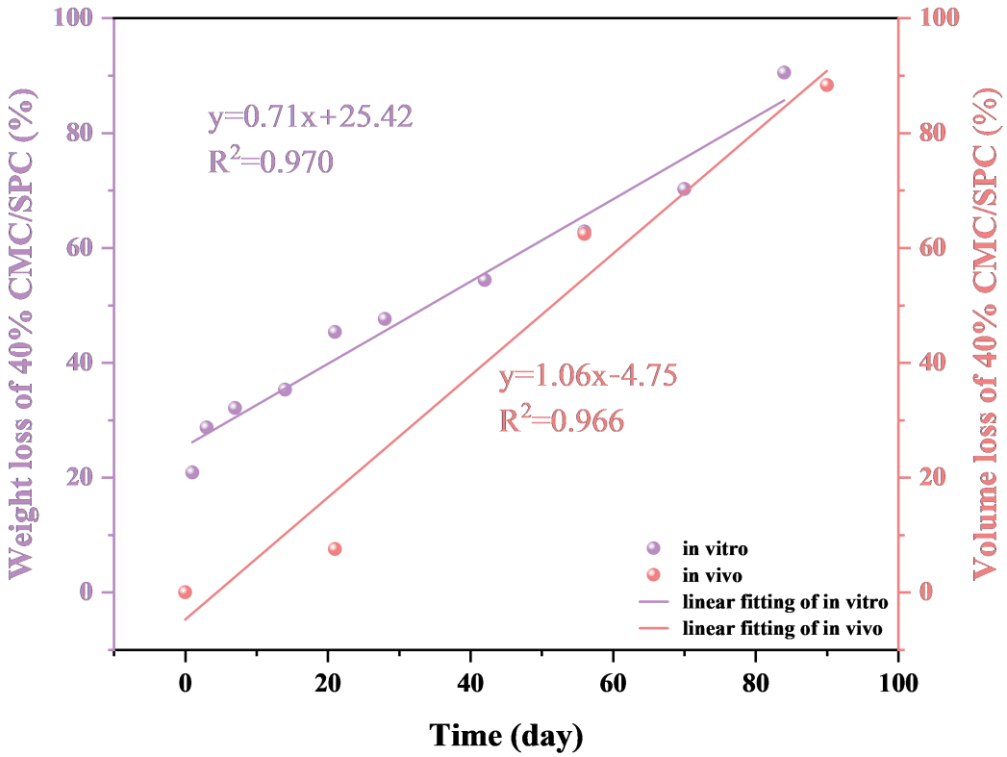

Figure S10. Comparison of in vivo and in vitro degradation for 40%CMC/SPC cement.

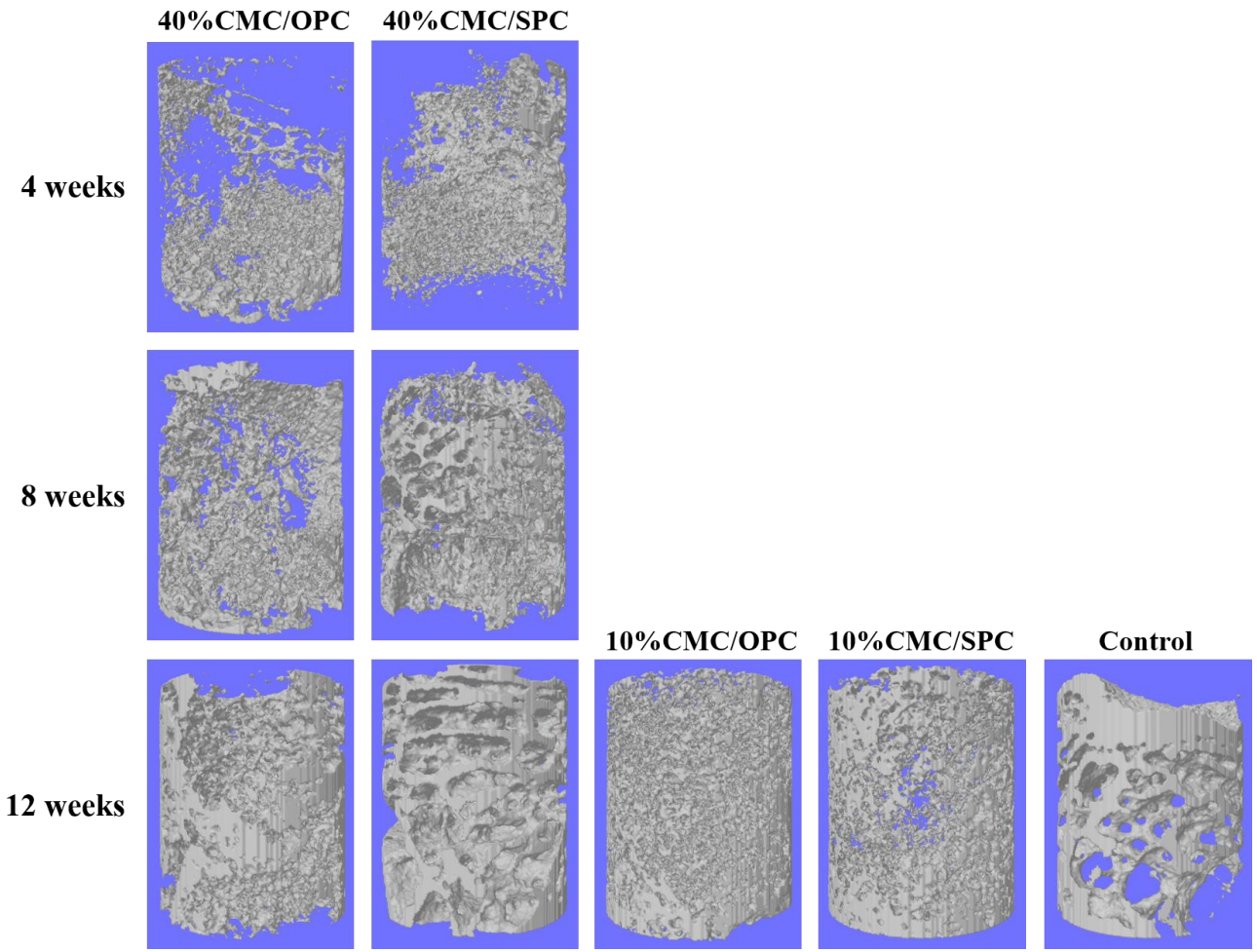

Figure S11. Reconstructed micro-CT images of the bone defect region at 4, 8, and 12 weeks.

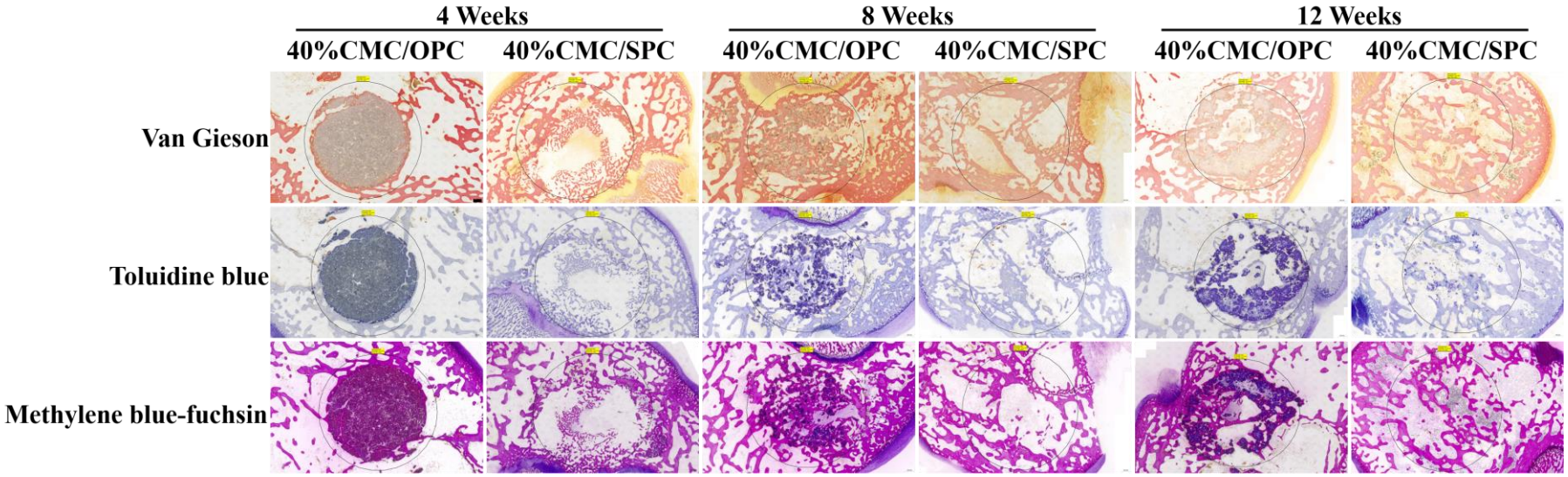

Figure S12. Van gieson, toluidine blue, and methylene blue-fuchsin staining for bone tissue around different implants (scale bar: 500 μm, black circles represent the area of bone defects).

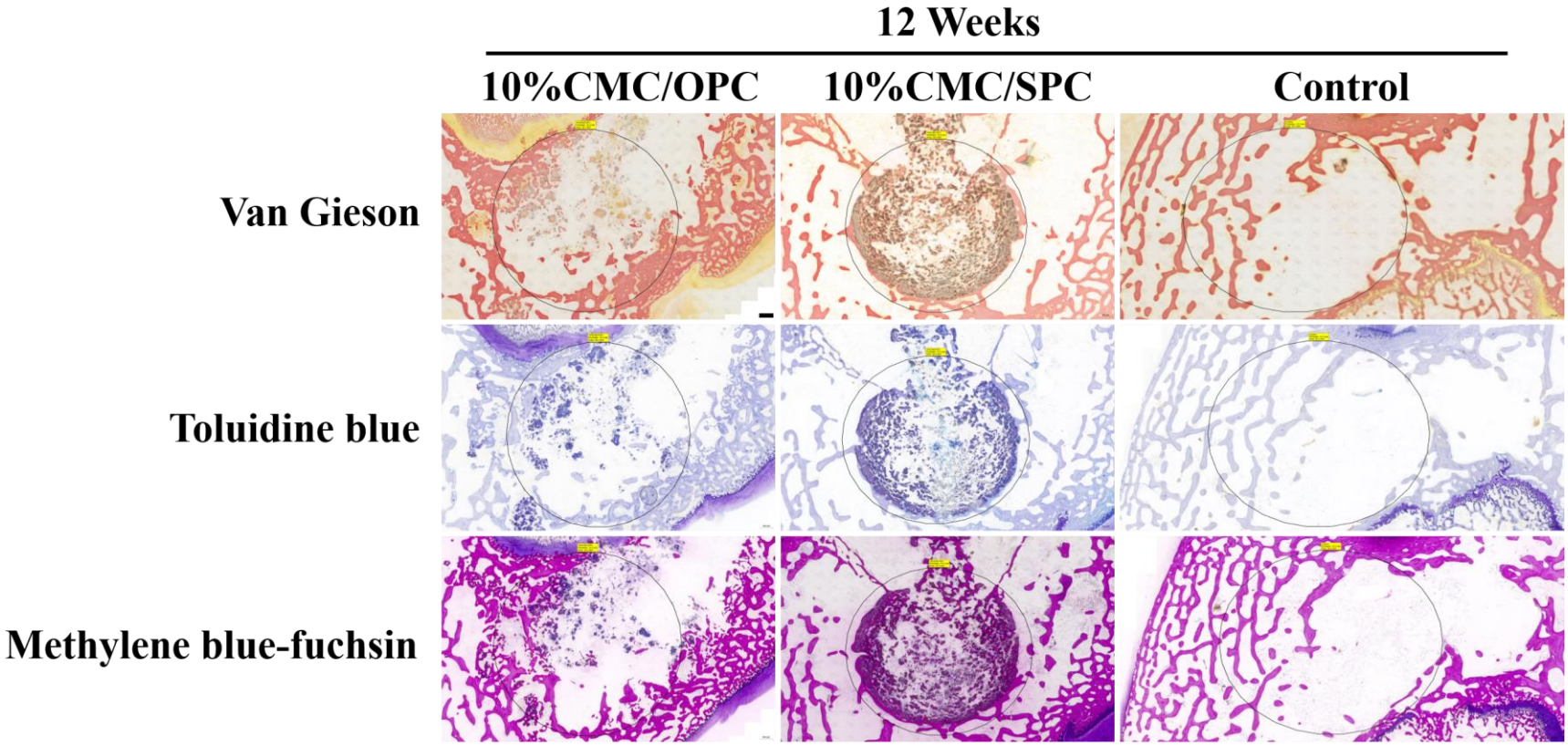

Figure S13. Van gieson, toluidine blue, and methylene blue-fuchsin staining for bone tissue around different implants (scale bar: 500 μm, black circles represent the area of bone defects).

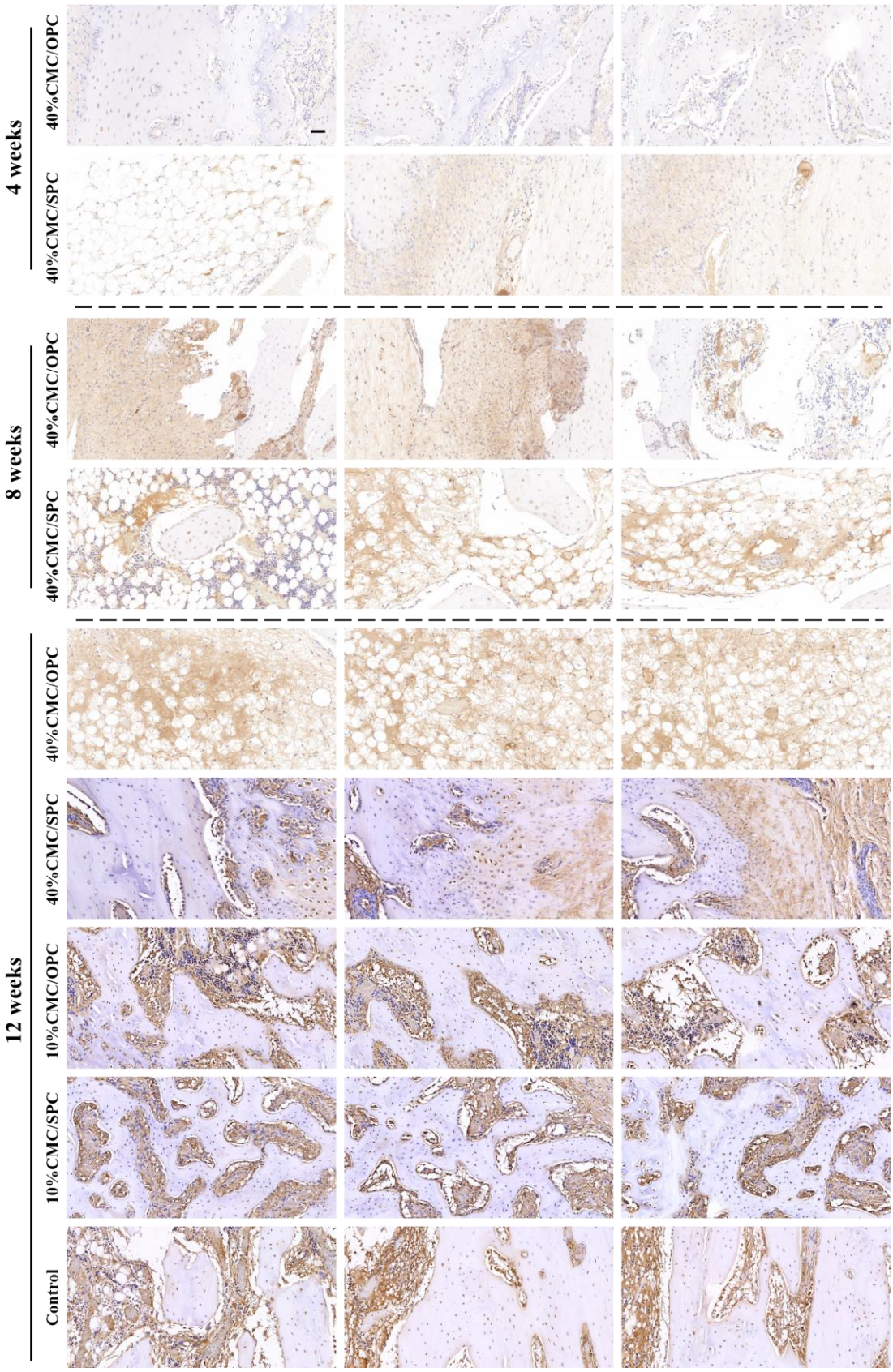

Figure S14. **Immunohistochemical staining of VEGF (scale bar: 50 μm).**

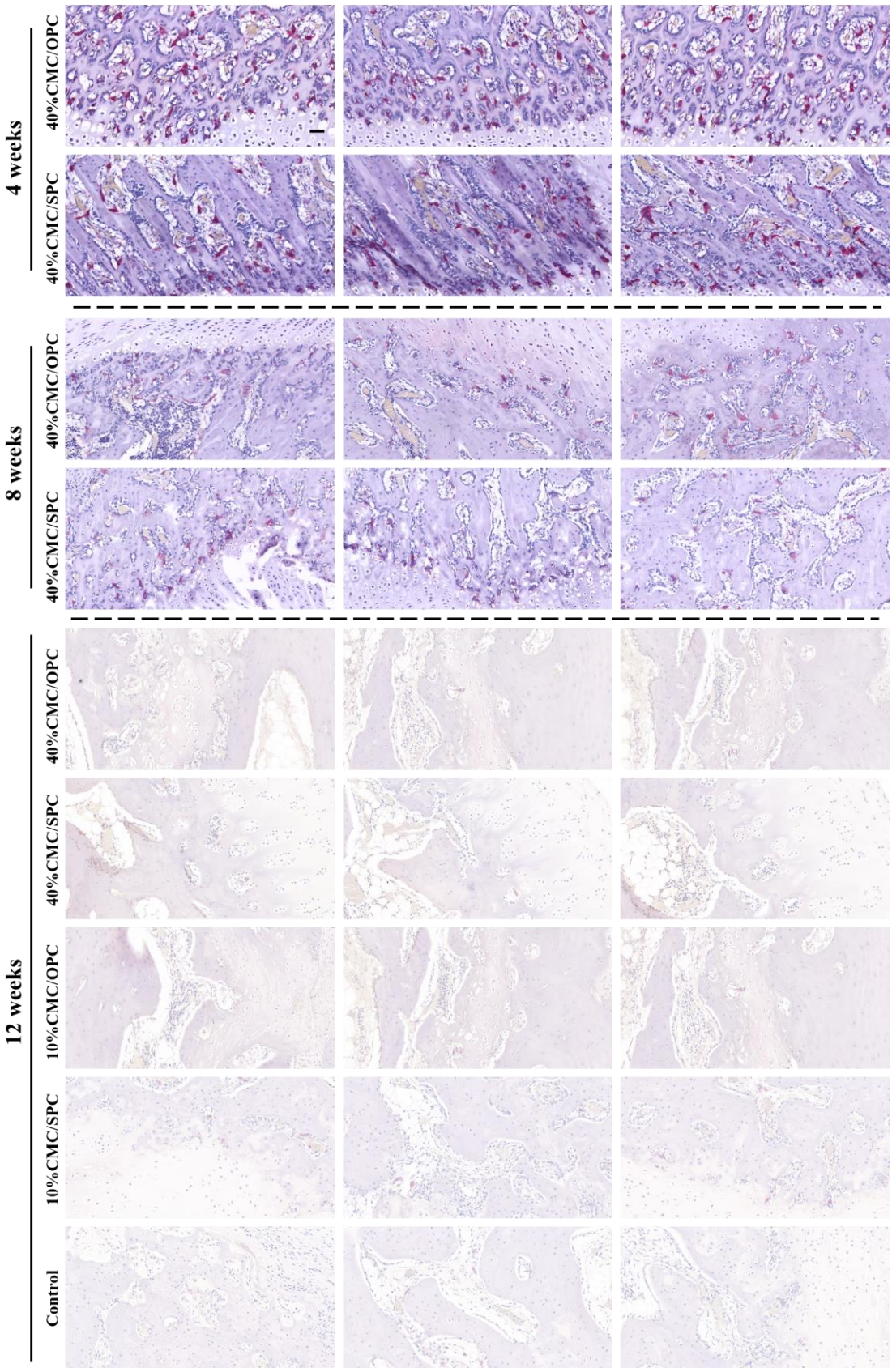

Figure S15. **Immunohistochemical staining of TRAP (scale bar: 50 μm).**

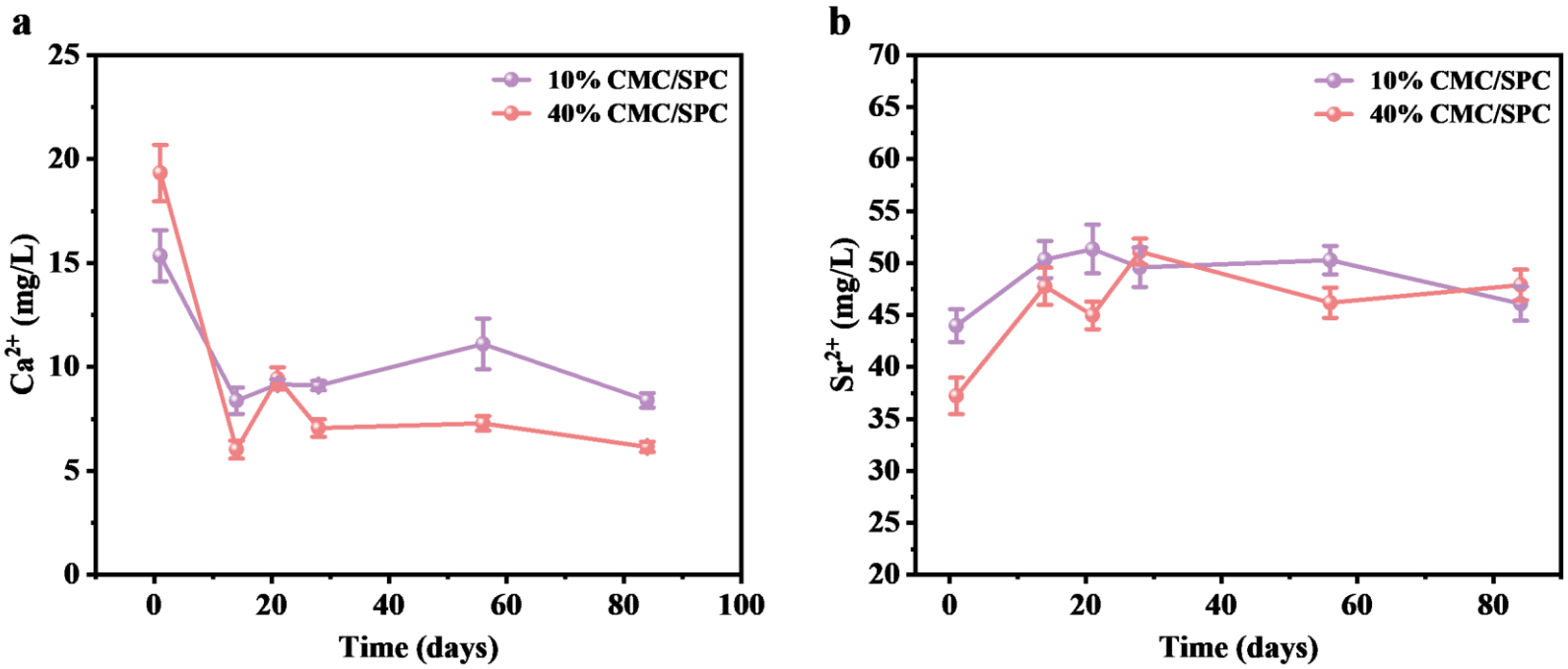

Figure S16. The variation of Ca^{2+} and Sr^{2+} concentration in PBS during the degradation process.

Figure S16a shows that the Ca^{2+} concentration dropped from 15–20 mg/L to 5–10 mg/L during the first two weeks. This is because $CaSO_4$ gradually decreased as it degraded, and Ca^{2+} could only be derived from the less soluble $CaHPO_4$ or Ca_3PO_4. After 20 days, the Ca^{2+} concentration stabilized at around 10 mg/L. Figure S16b shows an increase in Sr^{2+} concentration during the first two weeks, which is due to the fact that the K_{sp} of $SrSO_4$ is greater than that of $CaHPO_4$ or Ca_3PO_4. After 20 days, the Sr^{2+} concentration stabilized at around 47 mg/L.

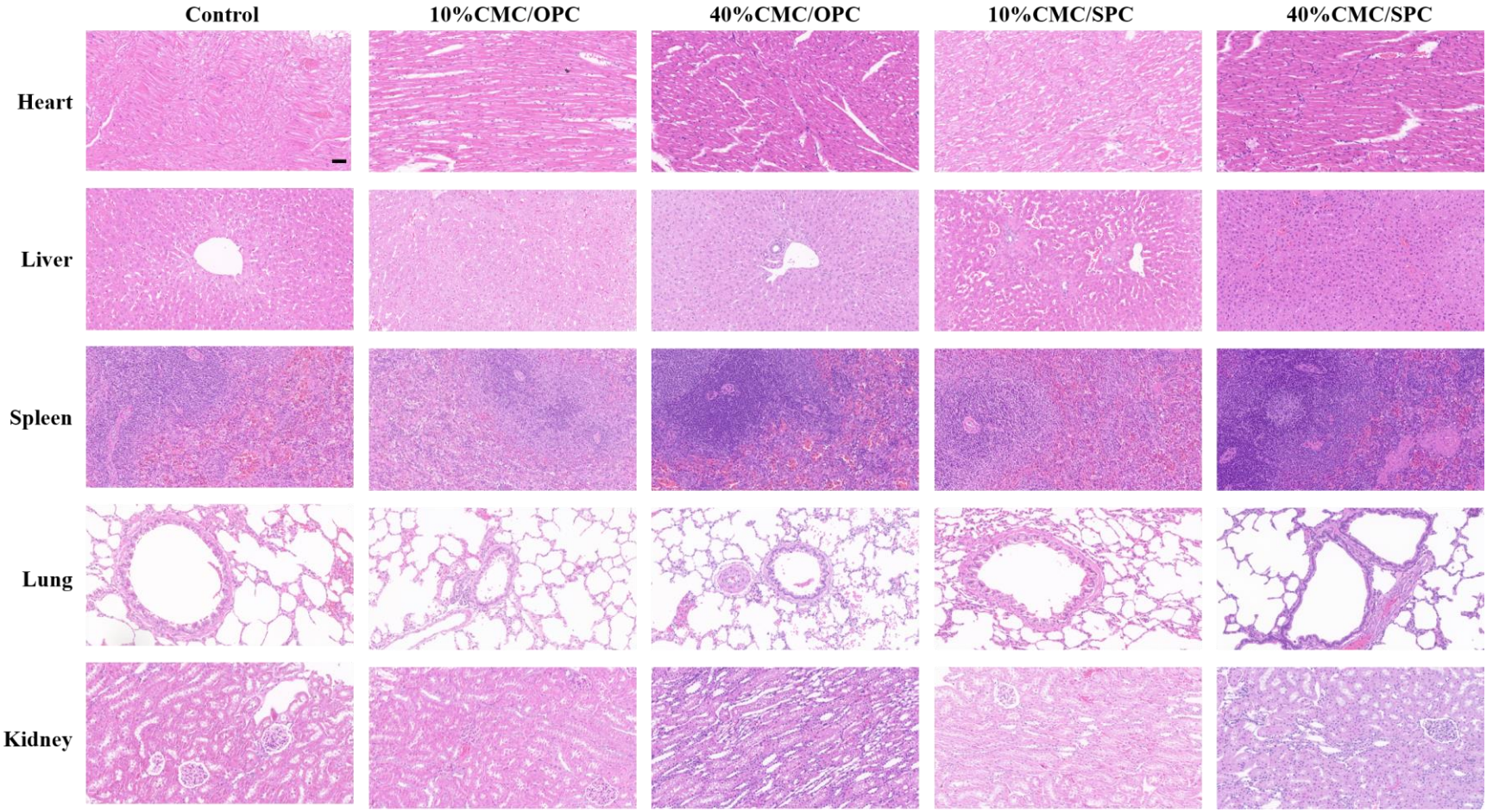

Figure S17. H&E staining images of major organs (scale bar: 50 μm).

2. Supplementary Tables

Table S1. Physicochemical properties and biological activity of different Sr-containing bone cements

Materials	Compression strength (MPa)	Degradation (%)	Injectability (%)	Setting time (min)/ curing temperature (℃)	Bioactivity
Sr-HA[1]	–	–	–	8-12/65	Promoting angiogenesis and bone tissue formation
Sr-BC[2]	17-25	–	40-100	7	–
SrCPC[3]	13-23	–	–	3-7	Inducing apatite deposition
SrCaHA[4]	–	–	–	1-30	–
SrO-CPC[5]	38-60	20 (60 d)	–	10-15	–
CGRP-Sr-CPC[6]	15-30	12 (28 d)	–	–	Upregulating ALP, BMP2, OCN, and Runx2 expression
Sr-BCPC[7]	9-38	2 (28 d)	–	9-20	Promoting the proliferation of MC3T3-E1 cells
Sr-BCs[8]	–	–	–	–	Inducing MCS and MC3T3-E1 cells Inhibiting osteoclast activity
Sr-CPC-O[9]	15-35	–	–	15-45	–
Rg_1-Sr-TiO_2/PP[10]	21/41	–	–	–	Promoting angiogenesis

mSCS-A[11]	3-6	–	65-95	–	Supporting hBMSC proliferation and osteogenesis differentiation
Sr-HA[12]	–	–	–	–	Increasing OCN/Runx2 expression and bone formation
SIS/SrFeHA[13]	–	–	–	–	Inducing angiogenesis/osteogenesis both in vitro and in vivo
SrCS/SF[14]	–	8 (14 d)	–	–	Promoting the osteogenic and angiogenic activities
Sr+Ma-BrC[15]	–	–	–	8-12	Promoting new bone formation
SrCSH/Sr-TCP[16]	–	–	–	–	Supporting the proliferation, adhesion, and ALP activity of MC3T3-E1, matching the growth rate of new bone
Sr-TCP[17]	13	–	–	–	Cytocompatibility for NCTC 3T3 and human DPSC cells
Sr-CS[18]	–	25 (56 d)	–	–	Appreciable biodissolution and high osteogenic capacity
HA-SrMg[19]	–	–	–	33-39	Increasing ALP and NO production
Sr/Cu-BSG[20]	11-15	37 (21 d)	88-94	14-23/31	Regulating inflammation, angiogenesis, and osteogenesis
Sr-CS/CPC[21]	16-21	14 (28 d)	96-98	16-40	Enhancing osteogenesis and angiogenesis
MPC_$SrHPO_4$[22]	–	9 (56 d)	78-85	18-21	–
TCP-4Sr/CSH[23]	10-14	13 (56 d)	23-100	5-17	accelerating the biodegradation rate and new bone regeneration
CS-BG[24]	4	–	–	20-150	improving mineralization of the extracellular matrix

CSH/Sr-MBG-SG[25]	4-17	68 (28 d)	75-100	57-96	Inducing apatite deposition
Csi@HT[26]	5-9	28 (28 d)	–	–	Stimulating osteogenic potential
Zn/Sr-CS/CPC[27]	15-20	17 (28 d)	65-85	32-45	Stimulating osteogenesis-related genes (ALP, Runx2, COLI, OCN, and OPN) and angiogenesis-related genes (VEGF, bFGF, and eNOS)
SrR/PA-MOC[28]	20-100	20 (28 d)	–	–	Improving the ALP expression and new bone formation
Mg-Sr-CS[29]	7-12	11 (28 d)	–	14-16	Promoting the in vitro osteogenesis and angiogenesis
$C_2S(2P_6)C_2S$/Sr[30]	–	–	–	–	Increasing COLI, Runx2, OCN and ALP expression
This work (40%CMC/SPC)	66	88 (90 d)	98	50/35	Supporting mBMSC proliferation and osteogenesis differentiation Increasing COLI, Runx2, OCN and ALP expression Triggering macrophage polarization towards M2 Inhibiting osteoclast activity Promoting new bone formation

Table S2. Composition of SBF (1000 mL) used in the apatite mineralization study.

	NaCl	$NaHCO_3$	KCl	$K_2HPO_4 \cdot 3H_2O$	$MgCl_2 \cdot 6H_2O$	1.0 M HCl	$CaCl_2$	Na_2SO_4	Tris	HCl
Amounts	8.035 g	0.355 g	0.225 g	0.231 g	0.311 g	39 mL	0.292 g	0.072 g	6.118 g	0~5 mL
Purity (%)	⩾99.5	⩾99.5	⩾99.5	⩾99.0	⩾98.0	-	⩾96.0	⩾99.0	⩾99.5	-

Table S3. Primer sequences for RT-PCR.

Genes	ID	Direction	Sequences
GAPDH	**14433**	FORWARD	GGTTGTCTCCTGCGACTTCA
		REVERSE	TGGTCCAGGGTTTCTTACTCC
COL1	**12842**	FORWARD	TAAGGGTCCCCAATGGTGAGA
		REVERSE	GGGTCCCTCGACTCCTACAT
Runx2	**12393**	FORWARD	CCTTCAAGGTTGTAGCCCTC
		REVERSE	GGAGTAGTTCTCATCATTCCCG
OPN	**20750**	FORWARD	AAACACACAGACTTGAGCATTC
		REVERSE	TTAGGGTCTAGGACTAGCTTGT
OCN	**12096**	FORWARD	CAAGCAGGAGGGCAATAAGGTAGTG
		REVERSE	CGGTCTTCAAGCCATACTGGTCTG
***β*-Actin**	**11461**	FORWARD	GTGCTATGTTGCTCTAGACTTCG
		REVERSE	ATGCCACAGGATTCCATACC
iNOS	**18126**	FORWARD	ACTCAGCCAAGCCCTCACCTAC
		REVERSE	TCCAATCTCTGCCTATCCGTCTCG
Arg	**11846**	FORWARD	CATATCTGCCAAAGACATCGTG
		REVERSE	GACATCAAAGCTCAGGTGAATC

Table S4. Atomic percentages of different elements for the white rectangular region in Figure 1c.

Elements	$CaSO_4 \cdot 2H_2O$	$CaSO_4 \cdot 1/2H_2O$	Sr-HA	$SrSO_4$	$CaHPO_4$	CMC
C	13.20	11.53	15.65	48.19	19.91	55.76
O	60.87	50.57	43.92	30.02	56.17	33.35
Na	0.22	0.18	-	-	0.88	6.13
P	2.78	6.34	11.10	0.83	11.25	1.99
S	10.18	12.13	5.06	11.42	0.49	0.41
Ca	11.98	17.89	9.59	0.26	10.14	1.41
Sr	0.78	1.36	14.68	9.28	1.16	0.73

3. References

1. C. T. Wong, W. W. Lu, W. K. Chan, K. M. C. Cheung, K. D. K. Luk, D. S. Lu, A. B. M. Rabie, L. F. Deng and J. C. Y. Leong, Journal of Biomedical Materials Research Part A, 2004, 68A, 513-521.
2. S. Pina, P. M. C. Torres and J. M. F. Ferreira, Journal of Materials Science: Materials in Medicine, 2010, 21, 431-438.
3. S. Pina, P. M. Torres, F. Goetz-Neunhoeffer, J. Neubauer and J. M. F. Ferreira, Acta Biomaterialia, 2010, 6, 928-935.
4. D. Guo, M. Mao, W. Qi, H. Li, P. Ni, G. Gao and K. Xu, Journal of Materials Science: Materials in Medicine, 2011, 22, 2631-2640.
5. Y. Tao, D. Li and Y. Li, Journal of Wuhan University of Technology-Mater. Sci. Ed., 2013, 28, 741-745.
6. W. Liang, L. Li, X. Cui, Z. Tang, X. Wei, H. Pan and B. Li, Journal of Applied Biomaterials & Functional Materials, 2016, 14, 431-440.
7. H. Zhu, D. Guo, W. Qi and K. Xu, Biomedical Materials, 2017, 12, 015016.
8. M. Montesi, S. Panseri, M. Dapporto, A. Tampieri and S. Sprio, PLOS ONE, 2017, 12, e0172100.
9. T. Yu, S. Zeng, X. Liu, H. Shi, J. Ye and C. Zhou, Ceramics International, 2017, 43, 12579-12587.
10. M. Salarian, W. Z. Xu, R. Bohay, E. M. K. Lui and P. A. Charpentier, Macromolecular Bioscience, 2017, 17, 1600156.
11. M. Qiu, D. Chen, C. Shen, J. Shen, H. Zhao and Y. He, RSC Advances, 2017, 7, 23671-23679.
12. C. Huang, D. Li, J. Song, K. Chen, X. Wang, F. Zhao, X. Gu, X. Xie and Y. Fan, Applied Materials Today, 2023, 30, 101723.
13. W. Cui, L. Yang, I. Ullah, K. Yu, Z. Zhao, X. Gao, T. Liu, M. Liu, P. Li, J. Wang and X. Guo, Biomedical Materials, 2022, 17, 025008.
14. Y. Zhou, Y. Hu, M. Uemura, L. Xia, X. Yu and Y. Xu, Frontiers in Bioengineering and Biotechnology, 2022, 10, 842530.
15. S. K. Nandi, M. Roy, A. Bandyopadhyay and S. Bose, Journal of Biomedical Materials Research Part B: Applied Biomaterials, 2023, 111,

599-609.

16. Q. Miao, N. Jiang, Q. Yang, I. M. Hussein, Z. Luo, L. Wang and S. Yang, Biomedical Materials, 2022, 17, 015014.

17. J. V. Rau, I. V. Fadeeva, A. A. Forysenkova, G. A. Davydova, M. Fosca, Y. Y. Filippov, I. V. Antoniac, A. Antoniac, A. D'Arco, M. Di Fabrizio, M. Petrarca, S. Lupi, M. Di Menno Di Bucchianico, V. G. Yankova, V. I. Putlayev and M. B. Cristea, Advanced Materials Interfaces, 2022, 9, 2200803.

18. Y. Cong, Z. Liang, N. Jianping, H. Wenyue, G.-A. E. Prince and X. Zhang, Medical & Biological Engineering & Computing, 2022, 60, 1691-1703.

19. A. M. Dias, I. do Nascimento Canhas, C. G. O. Bruziquesi, M. G. Speziali, R. D. Sinisterra and M. E. Cortés, Biological Trace Element Research, 2023, 201, 2963-2981.

20. S. Li, L. Zhang, C. Liu, J. Kim, K. Su, T. Chen, L. Zhao, X. Lu, H. Zhang, Y. Cui, X. Cui, F. Yuan and H. Pan, Bioactive Materials, 2023, 23, 101-117.

21. T. Wu, T. Lu, H. Shi, J. Wang and J. Ye, Ceramics International, 2023, 49, 6630-6645.

22. R. Gelli, G. Bernardini and F. Ridi, Ceramics International, 2023, 49, 31466-31476.

23. H. Chen, M. Shen, J. Shen, Y. Li, R. Wang, M. Ye, J. Li, C. Zhong, Z. Bao, X. Yang, X. Li, Z. Gou and S. Xu, Biomaterials Advances, 2022, 141, 213098.

24. N. Moazeni, S. Hesaraki, A. Behnamghader, J. Esmaeilzadeh, G. Orive, A. Dolatshahi-Pirouz and S. Borhan, Biomedicines, 2023, 11, 2833.

25. F. Banche-Niclot, I. Corvaglia, C. Cavalera, E. Boggio, C. L. Gigliotti, U. Dianzani, A. Tzagiollari, N. Dunne, A. Manca, S. Fiorilli and C.

Vitale-Brovarone, Biomolecules, 2023, 13, 94.

26. Z. Bao, J. Yang, J. Shen, C. Wang, Y. Li, Y. Zhang, G. Yang, C. Zhong, S. Xu, L. Xie, M. Shen and Z. Gou, Journal of Materials Chemistry B, 2023, 11, 2417-2430.

27. X. Yuan, T. Wu, T. Lu and J. Ye, ACS Biomaterials Science & Engineering, 2023, 9, 5761-5771.

28. T. Ma, Y. Guan, J. Feng, Y. Yang, J. Chen, W. Guo, J. Liao and Y. Zhang, Biomaterials Research, 2023, 27, 128.

29. C.-Y. Wang, C.-Y. Chen, K.-H. Chen, Y.-H. Lin, T.-P. Yeh, A. Kai-Xing Lee, C.-C. Huang and M.-Y. Shie, Ceramics International, 2024, 50, 7121-7131.

30. J. Elango, K. Salazar, P. Velasquez, A. Murciano, P. N. de Aza, W. Wu, J. M. Granero Marín and J. E. Mate Sanchez de Val, Ceramics International, 2024, 50, 16998-17010.